

Self-assembly of spherical interpolyelectrolyte complexes from oppositely charged polymers

Vladimir A. Baulin,^{*a,b} and Emmanuel Trizac^c

Received Xth XXXXXXXXXX 20XX, Accepted Xth XXXXXXXXXX 20XX

First published on the web Xth XXXXXXXXXX 200X

DOI: 10.1039/b000000x

The formation of inter-polyelectrolyte complexes from the association of oppositely charged polymers in an electrolyte is studied. The charged polymers are linear oppositely charged polyelectrolytes, with possibly a neutral block. This leads to complexes with a charged core, and a more dilute corona of dangling chains, or of loops (flower-like structure). The equilibrium aggregation number of the complexes (number of polycations m_+ and polyanions m_-) is determined by minimizing the relevant free energy functional, the Coulombic contribution of which is worked out within Poisson-Boltzmann theory. The complexes can be viewed as colloids that are permeable to micro-ionic species, including salt. We find that the complexation process can be highly specific, giving rise to very localized size distribution in composition space (m_+, m_-).

1 Introduction

Electrostatic interactions are instrumental in determining the structure and function of living organisms, biopolymers and drug delivery systems. Charged macromolecules can self-assemble and aggregate into compact intermolecular complexes. This ability of oppositely charged polymers to form finite size complexes determines their biological function, which for example is important in gene transfection and compactization of DNA^{1–3}, that provide promising alternatives to viral vectors⁴. Such macromolecular systems, where electrostatic forces are usually stronger than van der Waals or hydrogen bonds, exhibit rich behavior and structural variability. The structures formed by opposite charges are usually more stable than neutral block copolymers micelles dissociating upon dilution or slight change in the external conditions. The concept of stabilization of intermolecular complexes by interaction of oppositely charged polymers is realized in interpolyelectrolyte or polyion complexes (PIC) and polyion complex micelles (PIC micelles) that can be used for drug delivery^{5–7}. High stability of PICs opens the possibility to use them as functional devices where the responsiveness to external stimuli can be connected with a function, e.g. recognition at the molecular level⁸, pH-sensitive switching devices⁹ or drug delivery carriers transporting charged objects through the cell membrane^{7,10}.

Polyion complexes have enhanced ability to undergo struc-

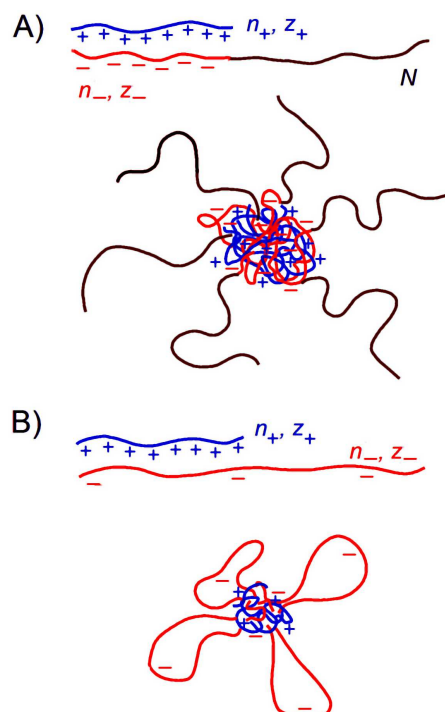


Fig. 1 Interpolyelectrolyte complexes formed by A) a linear polyelectrolyte (blue) and a diblock copolymer composed of an oppositely charged block (red) and a neutral block (black); upon assembling, these chains form the complex sketched, where the corona is made up of the neutral blocks; B) two linear oppositely charged polyelectrolytes (blue and red) with large asymmetry in the distances between charges (n_+ and n_-). The segments with non-compensated charges form a charged corona of loops.

^aICREA, Passeig Lluís Companys, 23 Barcelona, Spain E-mail: vladimir.baulin@urv.cat

^bDepartament d'Enginyeria Química, Universitat Rovira i Virgili, Av. dels Països Catalans, 26 Tarragona, Spain

^cUniversité Paris-Sud, Laboratoire de Physique Théorique et Modèles Statistiques, UMR CNRS 8626, 91405 Orsay, France

tural changes subject to external conditions, compared to neutral block copolymer assemblies. In addition to the response in change of temperature and solvent quality¹¹, the structure of the charged complexes can be very sensitive to changes in salt concentration^{12–15}, pH^{3,9,15,16}, charge ratio^{17,18}, addition of ions¹⁹, or mixing ratio^{2,20}. Tuning the molecular architecture and global properties of PICs would allow for precise control of their functional properties. Understanding the physics and fundamental features of the self-assembly of PICs is thus a challenging task. Oppositely charged polymers in symmetric solutions can precipitate into uniform macroscopic phase of polymers and ions^{21,22}. The physics of aggregated chains of opposite charge in precipitate is somehow similar to polyampholites, polymers containing both positive and negative charges dispersed along the chain²³. However, if the distribution of charges along the chain is not random²⁴ or one of the charged polymers is a diblock copolymer with a neutral block^{3,8}, oppositely charged polymers can form finite size complexes composed of a dense polyelectrolyte core and a swollen corona which protects the cores from aggregation by steric repulsion.

In this paper, we explore electrostatic properties and equilibrium structures of spherical complexes formed by oppositely charged polymers. The stability of finite size aggregates results from the balance of the electrostatic attraction between opposite charges in the core of the complexes and the steric repulsion of backbone segments forming a corona around the core. The description of such complexes is similar to polyelectrolyte micellization^{25–28}, combined with thermodynamics of aggregation in bidisperse solution^{29–32}. The steric repulsion in the corona should be strong enough to stabilize the complexes of finite size. This is possible when the hydrophilic blocks forming the corona of the complexes are long enough to oppose the electrostatic attraction in the core. In addition, the bare charge of the complexes can be screened by the ions of salt and counterions, thus changing the electrostatic forces and affecting the equilibrium properties of the complexes. The interplay of those effects will be studied considering two geometries, as sketched in Fig. 1:

- (case A) the building blocks are a linear uniformly charged polyelectrolyte and a diblock copolymer composed of a neutral block and a charged block of opposite charge. The charged blocks aggregate with the linear polyelectrolytes to form a complex with a core surrounded by a corona of neutral segments. This case is that of a “hairy” and neutral surrounding outside the charged core.
- (case B) the building blocks are two linear polyelectrolytes of opposite charge with a large asymmetry of the distances between the charges. The core of such complexes is composed of charged blocks of both signs, and

is surrounded by the corona of loops of the segments between the charges. The corona can be neutral (segments between neighboring charges along the chain) or slightly charged (tails or longer segments between distant charges). Compared to case A, the dangling “hair” are replaced by loops, that may bear an electric charge.

The paper is organized as follows. In section 2, we first consider case A, with a charged core decorated by neutral dangling hair. The electrostatics of the complexes is taken into account through the full Poisson-Boltzmann (PB) equation which is solved numerically and compared with the analytical expression of the linearized Debye-Hückel (DH) equation. Particular attention will be paid to the counter-ion uptake, where a significant quantity of charge can be “trapped” inside the core, thereby reducing the electric field created outside the complex. A second mechanism for charge reduction is ascribable to the non-linearity of Poisson-Boltzmann framework: non-linear screening effectively modifies the total core charge, leading in general to a reduced effective (or renormalized) quantity seen from a large distance³³. At this level of description, the dangling hair are not taken into account. The more complex situation where the charged core is surrounded by charged loops (case B) will be addressed in section 3. In turn, these results will be used in section 4 to discuss the complexation behaviour of oppositely charged polymers. Conclusions will finally be drawn in section 5. An appendix summarizes the main notations employed.

2 Charged core surrounded by neutral corona (case A)

2.1 The model and its three relevant charges

The simplest structure of a thermodynamically stable polyion complexes of finite size is a spherical core, containing all bare charges, surrounded by a neutral corona (Figure 1A). Such a complex can be formed, for example, by diblock copolymers containing neutral blocks^{3,6–8,17,24,34,35}. The electrostatic interactions between oppositely charged polyelectrolytes drive the formation of a dense core which is stabilized by the steric repulsion of neutral blocks forming swollen corona around the core. Even in such simple geometry, it is possible to tune the structure of the complex. Its size can be controlled by the lengths of the blocks, the density of charges, pH, the charge asymmetry, the salt concentration and solution properties.

Assuming that the linear polyelectrolyte is positively charged while the blocks of the diblock copolymer bear a negative charge, a linear polyelectrolyte is described by the number of charges on the chain z_+ , and the distance between the charges n_+ while the block copolymer is described by the number of charges z_- , the distance between the charges n_- ,

and the length of a neutral block, N . Hence, the length of the polyelectrolyte chain is n_+z_+ and the total length of a block copolymer is $n_-z_- + N$. Here, the lengths are expressed in units of a Kuhn length (assumed common to both cationic and anionic chains).

If all polyelectrolyte charges of both signs are buried in the core and the neutral blocks form the corona, the total "bare" charge of the core formed by m_+ linear polyelectrolytes and m_- block copolymer chains is

$$Z_1 = z_+m_+ - z_-m_- \quad (1)$$

We will assume in the subsequent analysis that this charge is uniformly spread over the globule of radius R_c , and therefore occupies a volume $4\pi R_c^3/3$. The counterions and the salt ions can penetrate into the core of radius R_c , and thus, screen the bare charge of the polymers. The resulting charge of the "dressed" core, Z_2 , is the charge of the core screened by small ions; assuming spherical symmetry, we have

$$Z_2 = 4\pi \int_0^{R_c} r^2 dr \rho(r) \quad (2)$$

where the total charge density $\rho(r)$ reads (in units of the elementary charge q)

$$\rho(r) = \frac{Z_1}{4\pi R_c^3/3} H(R_c - r) + c_\infty e^{-\beta q \varphi(r)} - c_\infty e^{\beta q \varphi(r)}. \quad (3)$$

In the above relation, $\beta = 1/kT$ is the inverse temperature, $\varphi(r)$ is the electrostatic potential and $H(R_c - r)$ denotes the Heaviside step function, equal to 1 inside and 0 outside the core. The first term on the right hand side of Eq. (3) stems from the polymeric matrix, that contributes to the charge density as a spherical uniform background. We assume here that the system is in osmotic equilibrium with a salt reservoir with equal densities c_∞ of labile cations and anions; the canonical situation, where the salt density in the system would be *a priori* prescribed, is amenable to a very similar treatment as the one presented here. From the reservoir ionic concentration, we define the Debye length $1/\kappa$ through $\kappa^2 = 8\pi\ell_B c_\infty$, where $\ell_B = \beta q^2/\epsilon$ is the Bjerrum length and ϵ is the solvent dielectric permittivity. In Eq. (3), the last two terms are for the labile micro-ions concentration. The corresponding exponential relation between the density profiles and the local electrostatic potential is typical of the PB (Poisson-Boltzmann) approximation³⁶ that will be adopted in the remainder. Within such a mean-field simplification, the electrostatic problem at hand is the following:

$$\begin{cases} \nabla^2 \varphi(r) = -\frac{4\pi}{\epsilon} q \rho(r) \\ \left. \frac{d\varphi}{dr} \right|_{r=0} = 0 \\ \left. \frac{d\varphi}{dr} \right|_{r \rightarrow \infty} = 0 \end{cases} \quad (4)$$

The charge of the "dressed" core Z_2 should be smaller than the "bare" charge Z_1 ³⁷, Eq. (1), because of counter-ion penetration inside the globule. However, the latter charge may be large enough to trigger significant non-linear screening effects, that translate into an effective (or renormalized^{33,38}) charge Z_3 that can be much smaller than Z_2 . To be more precise, in the weakly coupled limit where $Z_2 \rightarrow 0$ (where one also has $Z_1 \rightarrow 0$), it is possible to solve analytically Eq. (4), since it reduces to $\nabla^2 \varphi = \kappa^2 \varphi$ for $r > R_c$. The resulting DH (Debye-Hückel) potential reads, for $r > R_c$

$$\varphi_{DH}(r) = Z_1 \Theta(\kappa R_c) \frac{e^{-\kappa r}}{\kappa r}, \quad (5)$$

where Θ is a salt-dependent geometric prefactor; the complete solution will be provided below in section 2.2. To define the renormalized charge Z_3 , it is sufficient to note that beyond the linear Debye-Hückel regime, for an arbitrary charge Z_2 , Eq. (4) again takes the form $\nabla^2 \varphi \simeq \kappa^2 \varphi$, but at large distances r where φ becomes small. We consequently have, within the non-linear PB framework:

$$\varphi(r) \sim Z_3 \Theta(\kappa R_c) \frac{e^{-\kappa r}}{\kappa r} \quad \text{for } r \rightarrow \infty. \quad (6)$$

By construction, $Z_3 \simeq Z_1$ in the Debye-Hückel regime, while $Z_3 \ll Z_1$ upon increasing Z_1 .

Introducing the dimensionless electrostatic potential $u(r) = \beta q \varphi(r)$ and dimensionless distance $x = r/R_c$, Eq. (4) in spherical polar coordinates is written in a dimensionless form

$$\begin{cases} u''(x) + \frac{2}{x} u'(x) = -3\tilde{Z}_1 H(1-x) + (\kappa R_c)^2 \sinh(u(x)) \\ u'(0) = 0 \\ u'(\infty) = 0 \end{cases} \quad (7)$$

There are then two dimensionless governing parameters, $\tilde{Z}_1 = Z_1 \ell_B / R_c$ and κR_c . The solution of this nonlinear equation gives the charge density and the distribution of small ions around the complex.

2.2 Two limiting cases: weak charges and salt-free situation

Equation (7) can be solved analytically in the DH approximation when the electrostatic potential is small, $u(x) \ll 1$. In this case, the charge density $\rho(x)$ can be linearized, $e^{\pm u(x)} \approx 1 \pm u(x)$, and the solution can be written in the form

$$u_{DH}(\kappa r) = \begin{cases} \vartheta \left[1 - (1 + \kappa R_c) \frac{e^{-\kappa R_c} \sinh(\kappa r)}{\kappa r} \right], & r < R_c \\ \vartheta [\kappa R_c \cosh(\kappa R_c) - \sinh(\kappa R_c)] \frac{e^{-\kappa r}}{\kappa r}, & r > R_c \end{cases} \quad (8)$$

where $\vartheta = 3\tilde{Z}_1/(\kappa R_c)^2$. As a consequence, the geometrical constant that enters into the electrostatic potential at large dis-

tances (5) is

$$\Theta(\kappa R_c) = \frac{3}{(\kappa R_c)^2} [\kappa R_c \cosh(\kappa R_c) - \sinh(\kappa R_c)]. \quad (9)$$

Our results for a charged polyelectrolyte complex in the presence of salt can be compared with the salt free regime³⁹. In this case, it is essential to enclose the complete system in a confining boundary, otherwise the counter-ions “evaporate” –their energy loss upon leaving the globule vicinity is outbeaten by the entropy gain of exploring a large volume– and the problem becomes trivial. We therefore define R_{WS} , the Wigner-Seitz radius³⁸ of a large sphere containing the system. We note that the ratio $\eta = (R_c/R_{WS})^3$ defines the volume fraction of globules in our system. In the present case where counterions only are present, the density of charges is

$$\rho(r) = \frac{3Z_1}{4\pi R_c^3} H(R_c - r) - c_0 e^{\beta q \phi(r)}, \quad (10)$$

where c_0 is a normalization parameter to ensure total electroneutrality (it does not have any physical significance as such, unless a particular “gauge” or reference has been chosen for the potential). A possible choice among others is $4\pi c_0 R_{WS}^3/3 = Z_1$. The corresponding dimensionless PB equation reads

$$\begin{cases} u''(x) + \frac{2}{x}u'(x) = -3\tilde{Z}_1 [H(1-x) - \eta e^{u(x)}] \\ u'(0) = 0 \\ u'(R_{WS}/R_c) = 0 \end{cases} \quad (11)$$

with re-scaled distance $x = r/R_c$. The dimensionless charge $\tilde{Z}_1 = Z_1 \ell_B/R_c$ and η are here independent control parameters.

2.3 Results

The solutions of the PB equation (7) for different dimensionless bare charge $\tilde{Z}_1 = Z_1 \ell_B/R_c$ are presented in Figure 2a). The comparison with DH approximation (8) shows as expected that this approximation is valid for weakly charged objects. Such a comparison is a test for the numerical procedure used to solve Eqs. (4), and of course, strong deviations are observed between DH and PB solutions for \tilde{Z}_1 larger than a few units. It is noteworthy in Fig. 2 that the electric potential inside the core tends to a plateau when Z_1 is high enough. The corresponding labile ion local charge indeed tends to compensate for the background charge, resulting in a vanishing total local charge density. This requirement implies that one has

$$u \rightarrow \text{arcsinh}[3\tilde{Z}_1/(\kappa R_c)^2], \quad (12)$$

which gives $u \rightarrow 3.91$ in Fig. 2a) for $\tilde{Z}_1 = 26$, and likewise $u \rightarrow 8.48$ in Fig. 2b) for $\kappa R_c = 0.18$, as can be seen.

The solution of the salt-free equation (11) is shown by a dotted line in Figure 2a). The absolute value of the corresponding electric potential u cannot be compared to its counterpart found with salt, but the variations of u can be. It can be seen on the figure, panel a), that the amplitude of u is as expected larger without salt (for the same value of \tilde{Z}_1). This illustrates the weaker screening without salt. In addition, panel b) shows that the small κR_c limit coincides with the salt-free limit, as it should (here, the salt-free solution has been shifted by the constant required to have the same potential at $r = 0$ as in the $\kappa R_c = 0.02$ case). The salt-free results reported here depend very weakly only on packing fraction.

The solution of the PB equation provides also the distribution of small ions around the core of the complex $\rho_{\pm}(r) = c_{\infty} e^{\pm u(r)}$. It is shown for different charges of the core \tilde{Z}_1 in Figure 3a) and fixed salt concentration c_{∞} in Figure 3b). As the charge is increased the concentration of small ions of opposite charge inside the core increases inducing stronger screening effect. The concentration of ions of both signs in the core increases with increase of the bulk concentration of salt. This is shown in Figure 3b), where the bare charge of the core \tilde{Z}_1 is fixed, while the concentration of salt in the solution is changed. If the salt concentration is low, the redistribution of small ions around the core is almost due to counterions and the concentration profile of small ions obtained from Eq. (7) approaches the corresponding salt free solution given by Eq. (11). In addition, the increase of salt concentration results in higher concentration and induces stronger redistribution of the small ions around the core.

The presence of small ions inside the complex impinges on the radial distribution of charges $\rho(r)$. The background “core” contribution to this quantity is a step function, while due to the penetration of labile ions, $\rho(r)$ is small in the globule center, where charge neutralization is most efficient, and increases upon increasing r (see Fig. 4). In addition, the charge density in the center of the core vanishes at high concentrations but also for large enough \tilde{Z}_1 .

The screening of the bare charge by small ions penetrating into the core can be measured by the charge of the “dressed” core, Z_2 introduced above in Eq. (2). The analytical expression for Z_2 can be obtained within the DH approximation: $\rho(r) = 3Z_1/(4\pi R_c^3) - 2c_{\infty} u_{DH}(\kappa r)$, where $u_{DH}(\kappa r)$ is given by Eq. (8). Thus,

$$\rho(r) = \frac{3Z_1}{4\pi R_c^3} (1 + \kappa R_c) e^{-\kappa R_c} \frac{\sinh(\kappa r)}{\kappa r}, r < R_c \quad (13)$$

from which it follows that

$$\frac{Z_{2DH}}{Z_1} = 3 \frac{1 + \kappa R_c}{(\kappa R_c)^3} (\kappa R_c \cosh(\kappa R_c) - \sinh(\kappa R_c)) e^{-\kappa R_c}. \quad (14)$$

It can be checked that this relation is consistent with the more

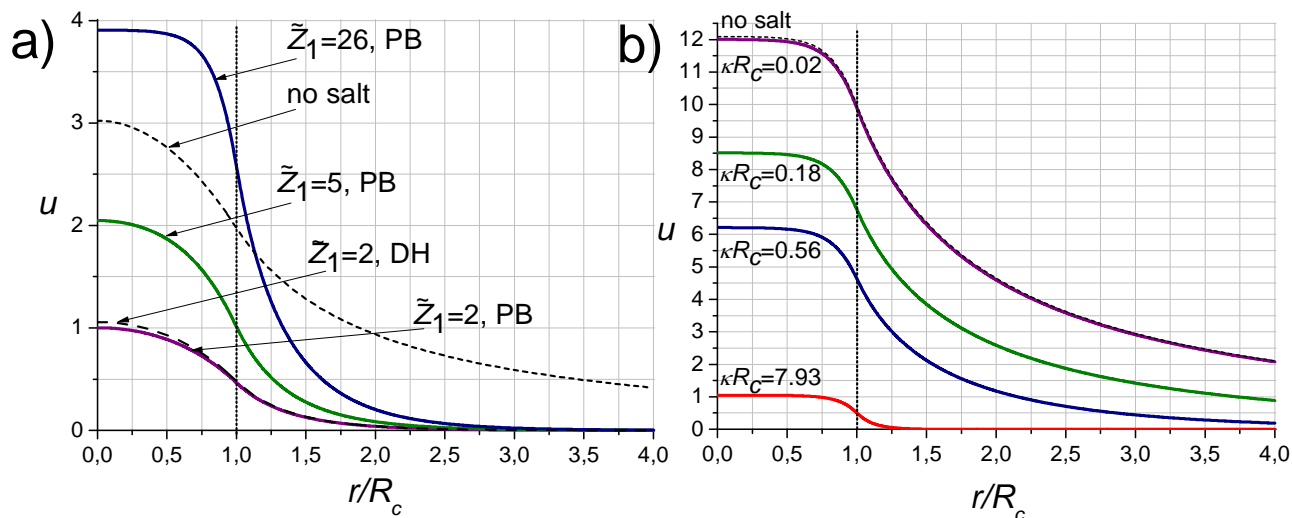


Fig. 2 a) Dimensionless electrostatic potential u as a function of the charge of the core \tilde{Z}_1 , for a fixed salt concentration corresponding to $\kappa R_c = 1.77$. b) Electrostatic potential u as a function of salt concentration. The charge of the core is fixed, $\tilde{Z}_1 = 26$. The dashed line is the solution of Eq. (11) with no salt, solid lines are the solutions of the non-linear PB equation (7), black dashed line is the solution of the DH equation (8), and the value of the packing fraction to solve the salt-free problem is $\eta = (R_c/R_{WS})^3 = 0.000125$.

familiar DH result for the potential of a spherical colloid having bare charge Z_2 and radius R_c ³³:

$$\varphi(r) = Z_2 \frac{e^{\kappa R_c}}{1 + \kappa R_c} \frac{e^{-\kappa r}}{r}, \quad (15)$$

which imposes that

$$\frac{Z_{2DH}}{Z_1} = \Theta(\kappa R_c) \frac{1 + \kappa R_c}{\kappa R_c} e^{-\kappa R_c} \quad (16)$$

From Eq. (14), we have that $Z_2 \propto Z_1$ within DH approximation, up to a salt-dependent prefactor. However, upon increasing Z_1 , non-linear effects become prevalent and invalidate the DH approach, see Fig. 5, obtained by solving the non-linear PB theory. The corresponding slower than linear increase of Z_2 with Z_1 is illustrated in Fig. 5a) and b), see also panel c) for the salt-free case. Increasing salt concentration screens out the charge, i.e. it leads to a decrease of Z_2 , and flattens the curves in panel a), where the DH prediction (14) holds for low \tilde{Z}_1 . In essence, increasing salt concentration ultimately leads to the DH limit where \tilde{Z}_2/\tilde{Z}_1 is Z_1 independent, as can be inferred from Eq. (8), where $u(0)$ is seen to decay with the increase of κ . A similar conclusion is drawn from expression (12): the DH limit is reached in the high salt limit. This trend is clearly seen in Fig. 5b), where all curves tend to collapse onto the DH behaviour for $\kappa R_c > 10$. On the other hand, \tilde{Z}_2/\tilde{Z}_1 is a strongly nonlinear function for large \tilde{Z}_1 in the no salt case. More precisely, it has been shown in Ref 39 that in the strongly non-linear salt-free regime, one has $Z_2 \propto Z_1^{1/2}$

(or equivalently $\tilde{Z}_2 \propto \tilde{Z}_1^{1/2}$). This prediction is successfully put to the test in Fig. 5c), which also shows that a change in the packing fraction $\eta = (R_c/R_{WS})^3$ does not affect the features discussed.

Finally, the behavior of the charged globule at large distances is encoded in the effective charge Z_3 , defined in Eq. (6), and therefore extracted from the far-field of the numerical solution to the non-linear equation (7). Such a quantity would rule the interactions between two distant globules. The corresponding plots of \tilde{Z}_3 are shown in Figure 6a) as a function of the globule charge for fixed salt concentration, and as a function of salt density for fixed background charge in Fig. 6b) and c). As is invariably the case in such mean-field approaches, the effective, or renormalized, charge increases upon increasing the bare charge^{33,38}. It also increases with salt concentration³³ and as imposed by the very definition of Z_3 , we find that $Z_3/Z_1 \rightarrow 1$ in the DH limit (enforced either from considering low \tilde{Z}_1 or large κR_c). In addition, Fig. 6b) shows that the ratio $Z_3/Z_2 = \tilde{Z}_3/\tilde{Z}_2$ is independent of bare charge Z_1 , except at very small salt concentrations. This reflects the fact that even for large Z_1 , counterion uptake is such that Z_2 is significantly reduced, and such that the colloid included internal salt ions can be treated by linearized mean-field theory. Indeed, it can be seen in Fig. 6b) that \tilde{Z}_3/\tilde{Z}_2 is close to its DH counterpart, given by $\tilde{Z}_1/\tilde{Z}_{2DH}$, see Eq. (14).

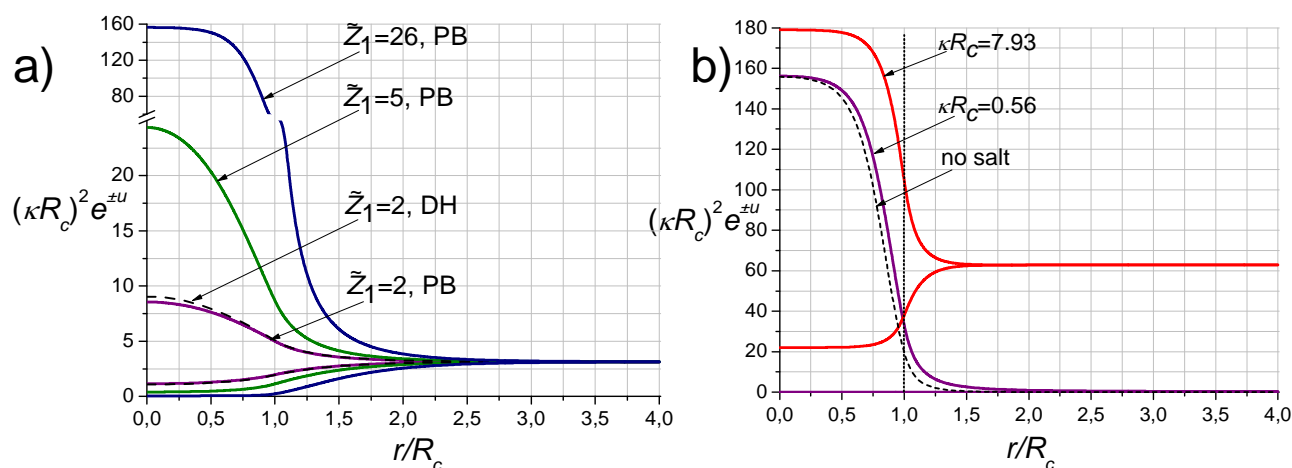


Fig. 3 Reduced density (up to a factor of two) of small ions around the core $\rho_{\pm} = c_{\infty} e^{\mp u(x)}$ a) for different charges of the core \tilde{Z}_1 and fixed salt concentration ($\kappa R_c = 1.77$) b) for different salt concentrations and fixed charge of the core ($\tilde{Z}_1 = 26$). For the no salt case, $\eta = 0.000125$.

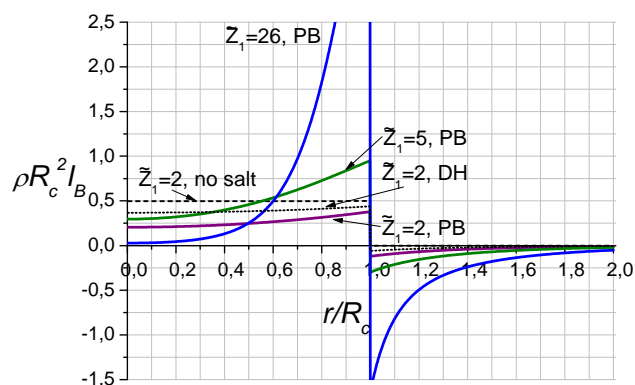


Fig. 4 Charge density $\rho R_c^2 l_B$ as a distance from the core for different charges of the core and fixed salt concentration $\kappa R_c = 1.77$. Here, $\eta = 0.000125$ for the no-salt result.

3 Charged core surrounded by charged corona (case B)

Thermodynamically stable polyelectrolyte complexes can also be formed by the complexation of two linear polyelectrolytes of opposite charge with a large asymmetry of the distances between the charges $\Delta = n_-/n_+ \gg 1$, which can form flower-like structures²⁴. The core of such complexes with a partially compensated charges is surrounded by a corona of long loops of a polymer with a longer distance between the charges (Fig. 1-B). The loops of size n_- , are neutral, but some larger loops and the tails can be charged.

Thus, we can generalize the discussion of the previous chapter to the case where the charged core is surrounded by a charged corona. We assume spherical symmetry in the dis-

tribution of the charges around the core, i.e. the charge in the corona depends only on the distance from the center of the core r . Since the charges in the loops and tails are attached to the core by polymer chains, the electrostatic interaction of those charges with the core is balanced by a weak entropic force due to polymer chain extension. If the electrostatic force is not very strong, a polymer chain carrying the charge can be envisioned as a Gaussian coil and the probability of radial distribution of charges is $P(r) \sim \exp\left[-\frac{3}{2na^2}(R_c - r)^2\right]$, where n is the length of the polymer chain in the corona and a is the Kuhn segment length. This approximation is valid for small charges that do not perturb significantly the statistics of the chains. The resulting density of charges is the sum of three terms: the bare charge of the core, the charge of the counter-

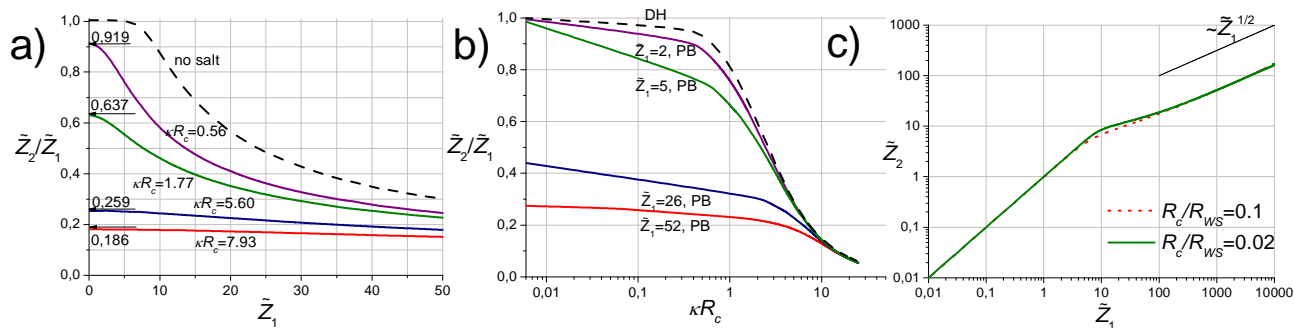


Fig. 5 Charge of the dressed core \tilde{Z}_2 (uptake charge) as defined in Eq. (2), as a function of a) bare charge for different salt concentrations b) salt for different values of bare charge \tilde{Z}_1 c) bare charge in the salt-free case, on a log-log scale. The arrows in panel a) show the Debye-Hückel prediction, Eq. (14), that provides the correct limiting behaviour at small charges. Note that in panel b), the Debye-Hückel prediction does not depend on \tilde{Z}_1 . The no salt solution in panel a) corresponds to $\eta = 0.01$ (which means $R_c/R_{WS} \simeq 0.21$).

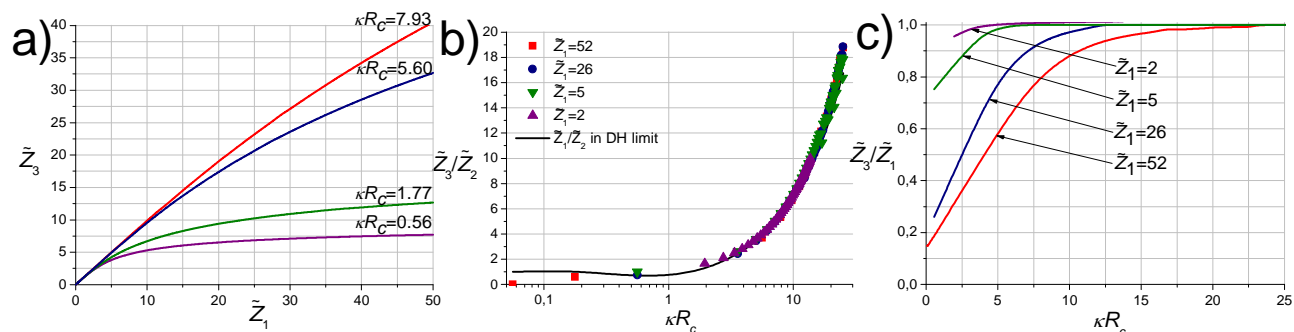


Fig. 6 a) Renormalized charge \tilde{Z}_3 of a globule as seen from large distances, as a function of the bare charge \tilde{Z}_1 for different salt concentrations. b) and c) show either Z_3/Z_2 or Z_3/Z_1 as a function of salt κR_c , for different bare charges. In panel b), the continuous curve is for the ratio Z_1/Z_2 found within DH approximation, which is thus the inverse of Eq. (14).

ons plus salt molecules, and the charge of the corona:

$$\rho(r) = \frac{3Z_1}{4\pi R_c^3 c_\infty} H(R_c - r) + c_\infty e^{-\beta q \phi(r)} - c_\infty e^{\beta q \phi(r)} + \rho_c P(r) e^{-\alpha \beta q \phi(r)} H(r - R_c) \quad (17)$$

where ρ_c , positive or negative, is a parameter controlling the total charge of the corona and $\alpha = \pm$ is the sign of this charge (+ when $\rho_c > 0$ and $-$ when $\rho_c < 0$). It was assumed here that all loops have the same length n and that ions in the corona are monovalent. This expression for $\rho(r)$ leads to a Poisson equation similar to Eq. (7).

Solution of Poisson's equation gives the radial distribution of the potential which is shown in Figure 7a) and 7b) for different charges of the corona. The charged corona influences the distribution of small ions around the core, a quantity that is displayed in Fig. 7c) and 7d). Weakly charged coronas clearly do not modify the monotonous decrease of u with distance that was observed in Fig. 2, but this is no longer the

case when ρ_c is increased. Indeed, a point where u reaches an extremum [maximum in panel a) and minimum in panel b)] can be observed. From Gauss theorem, this coincides with the point where the total integrated charge over a sphere having the corresponding radius vanishes. The physical phenomenon occurring in panel a) where the charges in the corona are of the same sign as the bare core (assumed positive), is that the positive corona induces a migration of negative micro-ions inside the core and its vicinity, that change the sign of the uptake charge Z_2 , which is now negative. Adding the corona charge to Z_2 , though, leads to a positive charge. Hence the charge inversion evidenced by the potential extremum. The density peak of negative micro-ions is clearly visible in panel c). On the other hand, when the bare core and the corona bear charges of opposite signs [panels b) and d)], a conjugate mechanism takes place: small labile cations are “sucked” inside by the core, which leads to an integrated charge in a running sphere that is positive for small spheres, and becomes negative once

it includes the corona. In all cases, the mechanism can be viewed as a corona induced local charge inversion.

We do not repeat the full analysis of the difference between bare, uptake, and effective charge in the present case, but we show how the total charge of the corona, $Z_{corona} = \int_{R_c}^{\infty} r^2 dr \alpha \rho_c P(r) e^{-\alpha \beta q \phi(r)} H(r - R_c)$, depends on the parameter ρ_c in Fig. 8.

4 Complexation of oppositely charged polymers

The previous sections, devoted to the electrostatics of polyelectrolyte complexes, have left aside the energetical aspects, to which we turn our attention hereafter. Once the total free energy of a given complex is known, it becomes possible to study the equilibrium behaviour, in particular the size distribution, of an initial “soup” of individual polycations and polyanions.

4.1 The total free energy and equilibrium complex size distribution

The size of the thermodynamically stable complexes of oppositely charged polymers is determined by the interplay of the steric repulsion of the chains in the corona and electrostatic attraction in the core. Thus, the formation of stable aggregates requires either long neutral blocks at least in one of the polyelectrolyte or a large asymmetry in the distances between the charges along the chain, e.g. $\Delta = n_-/n_+ \gg 1$. If the corona is composed of neutral blocks, the blocks should be long enough to stabilize the attraction in the core, if the corona is composed of loops between the charges, the segment n_- should be long and flexible enough to form a loop in the corona in the micelle.

Consider then a spherical polyion complex made up of two polyelectrolytes of opposite charge. Each complex is defined by the number of polycations, m_+ , and the number of polyanions, m_- . If we assume dense packing of the monomers in the core, the radius of the core R_c can be expressed in terms of the number of chains m_+ and m_- as $R_c = a \left[\frac{3}{4\pi} (N_+ m_+ + N_- m_-) \right]^{\frac{1}{3}}$, where a is the Kuhn segment, $N_{\pm} = n_{\pm} q_{\pm}$ are the lengths of the charged blocks (in units of a). The bare charge of the core Z_1 is then also expressed in terms of m_+ and m_- , see Eq. (1).

The distribution function of the polyion complexes c_{m_+,m_-} is the number concentration of the aggregates with given aggregation numbers m_+ and m_- . The total free energy of the solution of polyelectrolytes of opposite charge, their counterions and salt molecules is

$$\frac{F}{VkT} = \sum_{m_+,m_-=0}^{\infty} (c_{m_+,m_-} \ln [c_{m_+,m_-} v] - c_{m_+,m_-} + c_{m_+,m_-} F_{m_+,m_-}) \quad (18)$$

where V is the volume of the system, F_{m_+,m_-} is the free energy of the complex expressed in units of kT , v is a molecular volume associated with the de Broglie length. Minimization of this free energy^{29,30} with respect to c_{m_+,m_-} along with two conservation of mass conditions, fixing the total concentrations of polyanions, ϕ_- , and polycations, ϕ_+ ,

$$\phi_{\pm} = \sum_{m_{\pm}=0}^{\infty} m_{\pm} c_{m_+,m_-} \quad (19)$$

gives the equilibrium distribution of the aggregates by their size³²

$$vc_{m_+,m_-} = (vc_{1,0})^{m_+} (vc_{0,1})^{m_-} \exp \left[- (F_{m_+,m_-} - m_+ F_{1,0} - m_- F_{0,1}) \right] \quad (20)$$

The free energy of the complex F_{m_+,m_-} can be written as the sum of an electrostatic contribution, and a term accounting for the steric repulsion of tails/loops in the corona

$$F_{m_+,m_-} = \Omega_{el} + F_{corona}. \quad (21)$$

These two contributions are detailed below.

4.2 The electrostatic contribution

The electrostatic contribution Ω_{el} is related to the semi-grand potential Ω'_{el} , relevant to discuss the present situation which is canonical for the colloids (polymers), and grand-canonical for the salt entities (in osmotic equilibrium with a salt reservoir of density c_{∞}). The semi-grand potential accounts for electrostatic attraction between polyelectrolytes and small ions in the system as well as the entropic contribution of small ions around the complexes. We have⁴⁰

$$\Omega'_{el} = \int d\mathbf{r} \left\{ \frac{1}{2} q \rho(\mathbf{r}) \phi(\mathbf{r}) + kT \sum_{\alpha=\pm} \rho_{\alpha}(\mathbf{r}) \left(\ln \left[\frac{\rho_{\alpha}(\mathbf{r})}{c_{\infty}} \right] - 1 \right) \right\} \quad (22)$$

where the first term is the electrostatic energy of the ionic distribution, and the second term is the entropy associated with the translational movements of small ions. We note that the integral in Eq. (22) diverges for large systems (as it would also for neutral systems), so that we consider in the following the excess semi-grand potential with respect to reservoir

$$\Omega_{el} = \Omega'_{el} - \Omega_{el}^{reservoir} = \Omega'_{el} + \int d\mathbf{r} 2c_{\infty} \quad (23)$$

Thus, the excess potential Ω_{el} finally takes the form

$$\Omega_{el} = \int d\mathbf{r} \left\{ \frac{1}{2} q \rho(\mathbf{r}) \phi(\mathbf{r}) + kT \sum_{\alpha} \rho_{\alpha}(\mathbf{r}) \ln \frac{\rho_{\alpha}(\mathbf{r})}{c_{\infty}} - kT \sum_{\alpha} \rho_{\alpha}(\mathbf{r}) + 2c_{\infty} \right\} \quad (24)$$

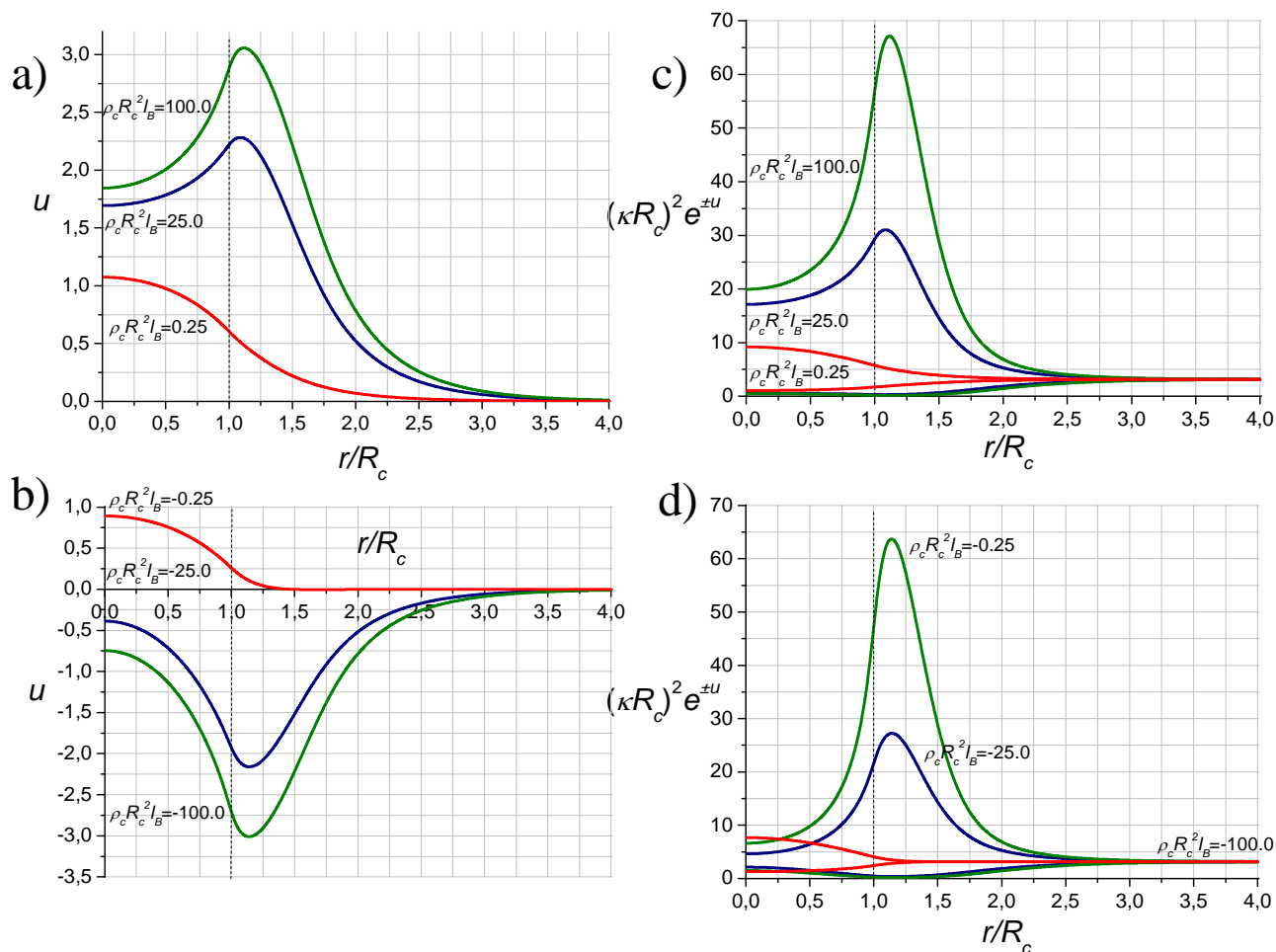


Fig. 7 Electrostatic potential $u(r)$ of the aggregate with a charged core $\tilde{Z}_1 = 2$, and a) a positively charged and b) a negatively charged corona. Distribution of small ions $(\kappa R_c)^2 e^{\pm u}$ around the positively charged core, $\tilde{Z}_1 = 2$, surrounded by c) positively charged and d) negative charged corona. Here $\kappa R_c = 1.77$, $R_c = 5a$ and $n = 5$.

For a spherical globule, this equation can be written in the dimensionless form as

$$\frac{\Omega_{el}}{kT} = 4\pi R_c^2 \ell_B \int_0^\infty x^2 dx \left\{ \frac{1}{2} \rho(x) u(x) + \rho_+(x) [-u(x) - 1] + \rho_-(x) [u(x) - 1] + 2c_\infty \right\} \quad (25)$$

where $x = r/R_c$ is the rescaled distance and we used the equality $\ln(\rho_\pm(x)/c_\infty) = \mp u(x)$. The analysis of the free energy of the charged complexes suggests that the complexes with charged corona of the same sign as the bare core have larger free energy than their neutral counterparts, and thus, are less favorable (Figure 9a)). However, if the charges of the core and the corona are opposite, the electrostatic energy can be lower (Figure 9b)).

The above applies for spherical globules, but leaves aside the particular cases ($m_+ = 0$, $m_- = 1$) and conversely ($m_+ = 1$,

$m_- = 0$), where the object to be considered is no longer a complex, but a polyanion or polycation respectively. We then need to adapt the previous arguments to these cases of an isolated charged chain in a salt solution. The polyelectrolyte chain is approximated as a cylinder of radius a with uniform linear charge density $\lambda_\pm \propto 1/n_\pm$, again treated within Poisson-Boltzmann theory. Introducing dimensionless distance $\tilde{r} = \kappa r$, where $\kappa^2 = 8\pi\ell_B c_\infty$, the corresponding PB equation in cylindrical coordinates yields, for an infinite cylinder

$$\begin{cases} \frac{1}{\tilde{r}} \frac{d}{d\tilde{r}} \left(\tilde{r} \frac{du}{d\tilde{r}} \right) = \sinh u \\ \frac{du}{d\tilde{r}} \Big|_{\tilde{r}=\kappa a} = \pm \frac{2\xi}{\kappa a} \\ u(\tilde{r} \rightarrow \infty) = 0 \end{cases} \quad (26)$$

Here $\xi = \ell_B \lambda_\pm$ is the so-called Manning parameter (dimen-

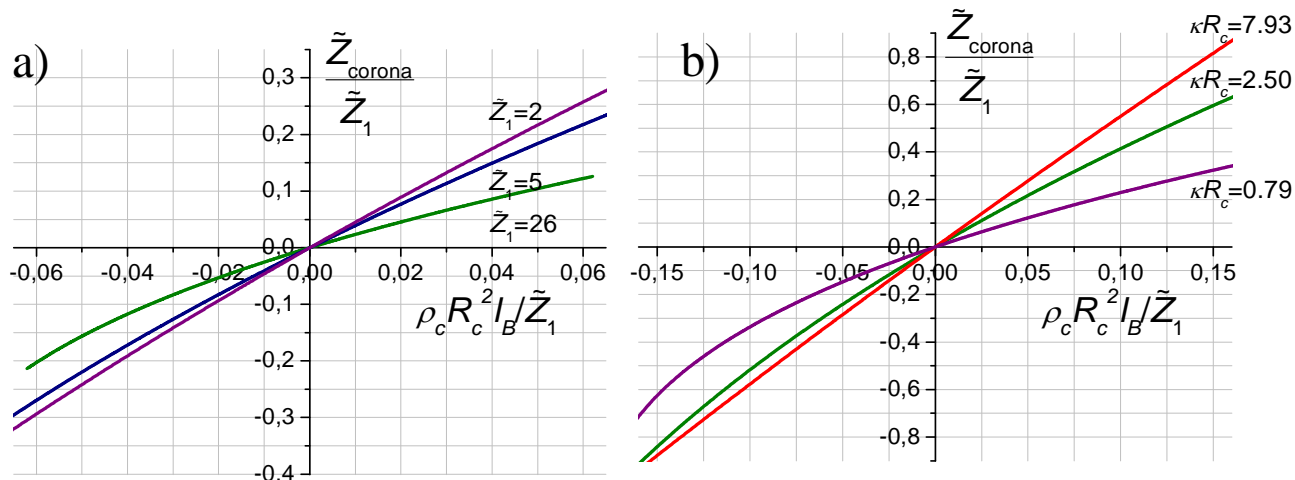


Fig. 8 Total charge of the corona $\tilde{Z}_{corona}/\tilde{Z}_1$ as a function of $\rho_c R_c^2 l_B$, a) the salt concentration is fixed, $\kappa R_c = 2.5$, b) the bare charge of the core is fixed, $\tilde{Z}_1 = 2$.

sionless line charge⁴¹). Once this equation has been solved, the electrostatic contribution to $F_{1,0}$ and $F_{0,1}$ for isolated chains of both signs follows from a similar calculation as that of Eq. (25):

$$\frac{\Omega_{el,\pm}^0}{kTN_{\pm}} = \frac{1}{2}u(0)\xi + \frac{1}{4}\int_{\kappa a}^{\infty} \tilde{r}d\tilde{r}u(\tilde{r})\sinh(u(\tilde{r})) - \frac{1}{2}\int_{\kappa a}^{\infty} \tilde{r}d\tilde{r}u(\tilde{r})[\cosh(u(\tilde{r})) - 1] \quad (27)$$

which was calculated per chain length N_{\pm} expressed in units of ℓ_B . In the following we assume that the Kuhn segment length of the polymer a is of the order of ℓ_B . Upon using the free energy of the infinite cylindrical macro-ion configuration, we neglect end effects, the consideration of which would be technically more involved.

Isolated chains, corresponding to $m_+ = 0$, $m_- = 1$ and $m_+ = 1$, $m_- = 0$ configurations are penalized by a large electrostatic energy $\Omega_{el,+}^0$ (see Figure 10). Indeed, these quantities bear a large self-term, notwithstanding the solvation phenomenon, that manifests itself in the fact that $\Omega_{el,+}^0$ decrease, for fixed charge ξ , upon addition of salt (i.e. increase of κa).

4.3 Steric repulsion of loops and tails

In the following, we consider a neutral and spherical polyelectrolyte complex made up of the charged core formed by oppositely charged polyelectrolytes and surrounded by the corona. We consider long tails and large loops in the corona, thus, the corona of the complex is then approximated by a star polymer (Fig. 1-A) or a flower structure (Fig. 1-B).

The electrostatic contribution (28) is balanced by the steric repulsion between the tails or loops in the corona. If the corona consists of long neutral blocks (star polymer, case A), this contribution is approximated by the free energy of a star polymer containing m_- arms of length N , which is the length of a neutral block. This approximation is valid when the core is much smaller than the corona and the arms are long enough to use the scaling expression⁴²

$$F_{corona} \sim -\ln N^{\sigma_{m_-} + m_- \sigma_1} \quad (28)$$

In this expression, σ_i are the universal exponents of the star polymers and their numerical values are calculated in Ref. 43.

If the corona consist of long neutral loops and tails (flower structure, case B), the free energy contribution is similar to (28), but the exponent is different,

$$F_{corona} \sim -\ln N^{\gamma_c - 1} \quad (29)$$

This exponent is calculated as follows. If the loops are formed by a single chain with p stickers joined together, $\gamma_c - 1 = \sigma_{2p} + 2\sigma_1 - (p-1)d\nu$, where the first term is the contribution of the center with $2p$ vertices, the second term is the contribution of the two tails and the last term is the contribution of $p-1$ loops. Each loop contributes with the Flory exponent ν in the dimension of the space d and is known numerically⁴⁴. If the loops are formed by m_+ chains with z_+ stickers and m_- chains with z_- stickers and all stickers are condensed on the core, the exponent is given by

$$\gamma_c - 1 = \sigma_{2z_+m_+ + 2z_-m_-} + 2\sigma_1(m_+ + m_-) - m_+(z_+ - 1)d\nu - m_-(z_- - 1)d\nu \quad (30)$$

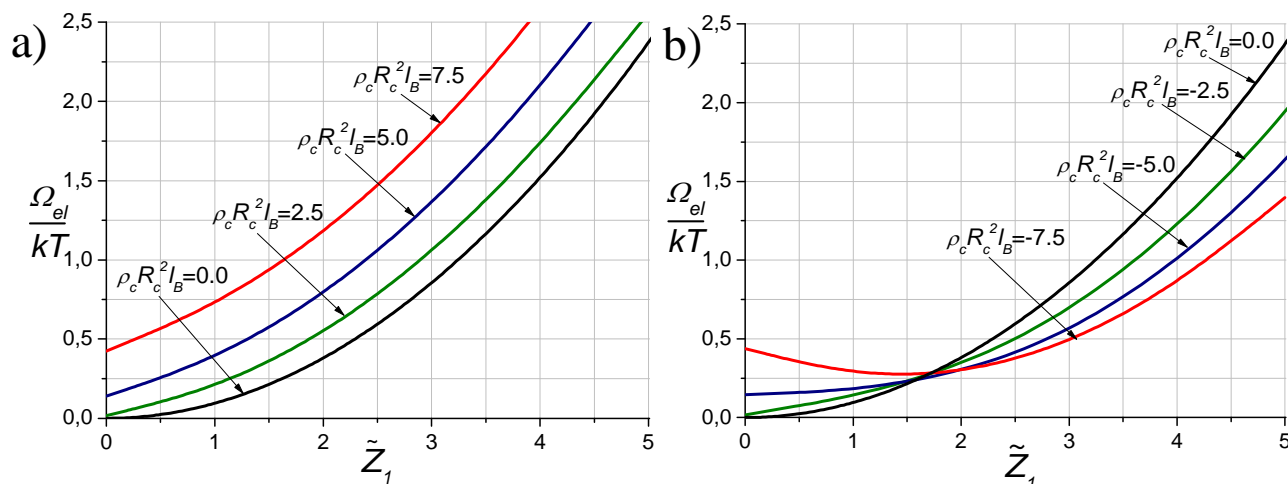


Fig. 9 Electrostatic excess energy Ω_{el} of a PIC with a) positively charged corona and b) negatively charged corona, as a function of the charge of the core, \tilde{Z}_1 , for a fixed salt concentration, $\kappa R_c = 7.93$.

Isolated non-aggregated polycations and polyanions are linear polymers, thus their entropy contribution is $F_{corona} \sim -\ln N^{2\sigma_1}$. Here we neglect the surface tension and hydrophobic interactions between polycations and polyanions in the core of the complexes, thereby assuming that the electrostatic attraction of opposite charges is the leading contribution; hydrophobic interactions may however be dominant for neutral complexes.

4.4 Results

Eq. (20) defines the equilibrium distribution function of the complexes c_{m_+, m_-} as a function of the geometry of the chains, asymmetry of the charges along the chain and salt concentration. We assume that the conformation of the polyelectrolyte complex is a spherical aggregate with a core formed by charged blocks surrounded by neutral corona (Figure 1-A)). Since the electrostatic contribution of the core and isolated chains in the solution is the main contribution to the free energy, one might expect that the thermodynamically stable complexes would be narrowly distributed in size and have the minimal possible charge. Thus, the equilibrium of the free energy would require the compensation of the charges inside the core, such that the formed PIC micelles are almost neutral. However, in our description we allow for deviations from zero charge, because other contributions to the total free energy, the entropy of mixing, the salt concentration and the steric repulsion in the corona, may shift the equilibrium.

The distribution function of the complexes, Eq. (20) is calculated for each combination of (m_+, m_-) and the results are shown in Fig. 11a). As an example, we plot the normalized vc_{m_+, m_-} for a mixture of a linear polymer with the

charge $z_+ = 18$ and oppositely charged diblock copolymer with a charged block, $z_- = 78$, and neutral block of length $N = 200$ (case A). The two polymers share the same distance between the charges along the chain: $n_+ = n_- = 1/\xi = 4$. It can be noted that all three distributions reported lie around the “electroneutrality line” $z_+ m_+ = z_- m_-$. In the vicinity of that line, the precise location of the support of the distribution function stems from a subtle balance of effects, as embodied in the free energy (18). We observe in Fig. 11b) that upon increasing the salt concentration, the equilibrium size distribution is shifted towards smaller complex sizes and becomes more peaked. For instance, for $\kappa a = 0.3$, the peak corresponds to $m_+ = 24$ and $m_- = 7$ (for which the complex has charge $z_+ m_+ - z_- m_- = -72$). A similar trend is observed while changing the length of the neutral block, which controls the repulsion in the corona. Long tails in the corona favor smaller complexes, and shift the equilibrium accordingly. Since the complexes are close to neutrality, the salt concentration mostly affects the electrostatic energy of free chains [Eq. (28)], and the shift of the aggregation numbers along the electroneutrality line is mainly due to the chains in the solution. In addition, increasing the bulk concentration of polymers, $vc_{1,0}$ and $vc_{0,1}$, increases the aggregation numbers, see Fig. 12.

Fig. 13 shows the size distribution function of the complexes formed by equally charged (“matched” in terms of Ref. 8) polymers (18,18), (44,44) and (78,78) and “unmatched” polymers, (18,78) and (78,18). The polymer concentrations are chosen in such a way that the complexes are formed close to the origin, which may indicate the onset of aggregation. Aggregation of long polymers, (78,78), occurs at smaller concentrations than aggregation of short polymers, (18,18), due

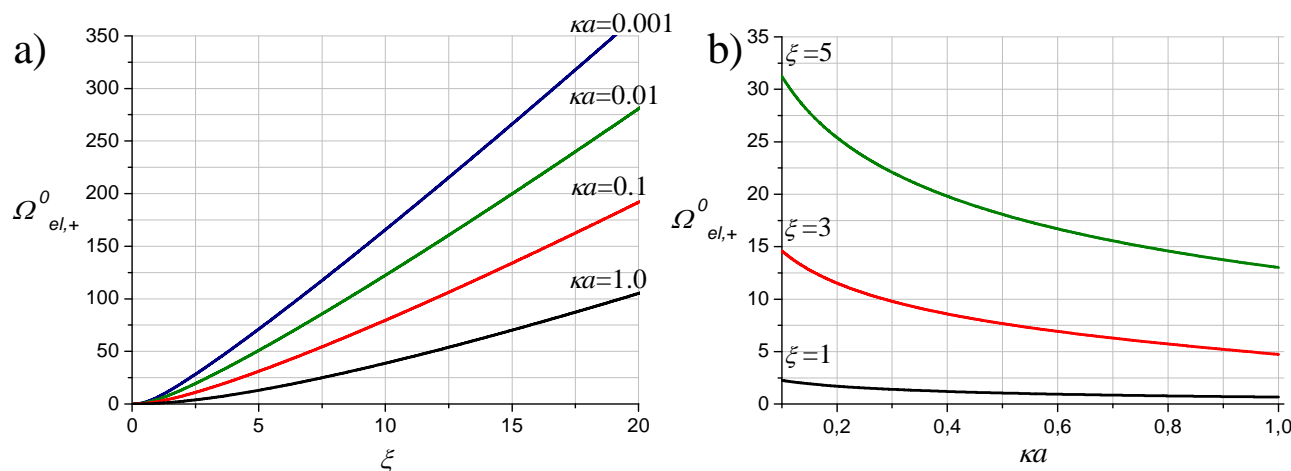


Fig. 10 Electrostatic energy $\Omega_{el,\pm}^0$ of the rod (Eq. 28) for the length ℓ_B as a function of a) the Manning parameter ξ (dimensionless linear charge) and b) salt concentration κa .

to the entropy of mixing, which strongly depends on the total length of polymers. We find that unmatched complexes [see the cases (18,78) and (78,18)], can also be formed if the aggregation numbers are close to the electroneutrality line (the opposite charges are compensated). On the other hand, Ref⁸ has put forward a chain recognition mechanism where matched cases are more prone to form large complexes, but the system considered there is somewhat different, involving the equilibrium between three types of individual chains together with two and three component complexes.

5 Discussion and conclusions

We have developed a framework to study the formation of polyelectrolyte complexes from an initial arbitrary mixture of charged polymers, where both polycations and polyanions are present in an electrolyte solution. Two situations were addressed, as sketched in Fig. 1: for a given polycation type, the polyanion is either a diblock copolymer with a long neutral tail (case A), or a polyanion having a different intercharge spacing along the backbone (case B). Coulombic attraction between oppositely charged polymers leads to the formation of complexes, with an *a priori* unknown composition. The numbers of chains of both types in a given complex were denoted m_+ and m_- . These complexes were envisioned as forming hairy structures, where the hair/corona is either made up of dangling neutral chains (case A) or of loops (case B), while the core of much smaller spatial extension contains most of the charges of the polymeric backbones. We started by focusing on the electrostatic aspects, treated at the level of Poisson-Boltzmann theory. This part of the work thereby extends a previous study performed for salt-free systems³⁹. In a second step, the re-

sulting electrostatic free energy of the complexes was used, together with the entropic repulsion between tails/loops in the corona, to provide us with a free energy functional for an arbitrary mixture of complexes having a given size distribution c_{m_+,m_-} . Upon minimizing this functional under the appropriate constraints of mass conservation for both polycationic and polyanionic species, we obtained the equilibrium composition of our mixture. Whereas this optimal distribution turns out to give a negligible weight to configurations that depart from complex global charge neutrality –a property that may have been anticipated–, it exhibits the non-trivial feature of a high selectivity: out of an initial random soup of polycations and polyanions, well defined complexes with precise composition (m_+ , m_-) may emerge, particularly when the salt density is increased.

The problem under study here is characterized by a large number of dimensionless parameters, and we furthermore made simplifying assumptions in the description, such as equating the Kuhn lengths for both positively and negatively charged polymers. We chiefly focused on the effect of changing the salt concentration, which is an experimentally simple control parameter. The pH dependence of the core charge of the complexes has not been addressed, but it can be incorporated for instance via the Henderson–Hasselbalch equation⁴⁵. In addition, the Coulombic aspects were treated at mean-field level, which is adequate provided the bare charge of the complex core, Z_1 , is smaller than a bound of order $[R_c/(z^2\ell_B)]^{3/4}$, which decreases when increasing the valence z of the mobile micro-ions (assumed here monovalent, i.e. $z = 1$). Finally, we have neglected the structure of the core, by homogeneously smearing out its charge. This certainly leads to overestimate their free energy, due to the neglect of the corresponding neg-

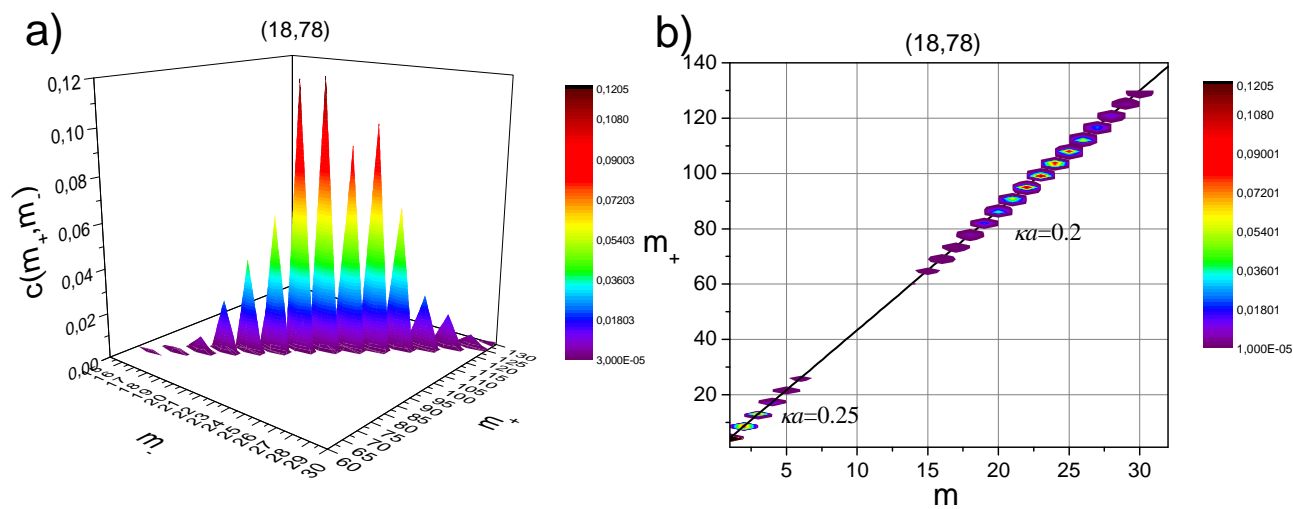


Fig. 11 Case A. a) Probability distribution function (normalized vc_{m_+,m_-}) for asymmetric block copolymers of opposite charge, $z_+ = 18$ and $z_- = 78$ with the same distance between the charges, and Manning parameter $\xi = 0.25$. The length of neutral block (stabilizing corona) is $N = 200$, the salt concentration is $\kappa a = 0.2$, and the concentrations of individual chains is $vc_{1,0} = 10^{-4}$ and $vc_{0,1} = 10^{-9}$. b) Projection of the same function on the plane (m_+, m_-) for three different salt concentrations.

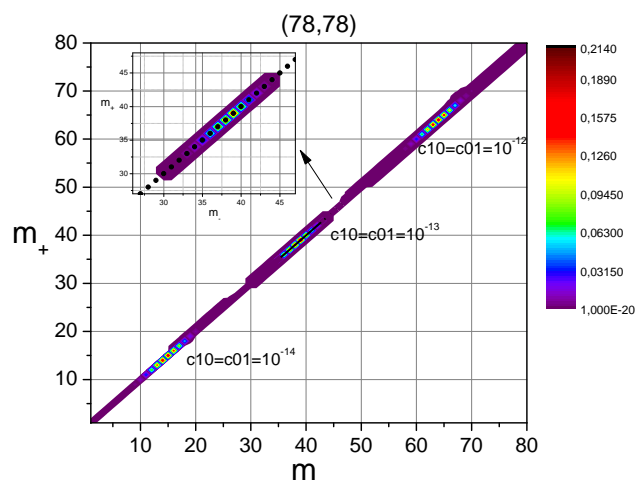


Fig. 12 Projections of the probability distribution function (normalized vc_{m_+,m_-}) on the plane (m_+, m_-) for the equally charged copolymers of opposite charges, $z_+ = 78$ and $z_- = 78$ as a function of polymer concentrations, $vc_{1,0}$ and $vc_{0,1}$. Manning parameter, $\xi = 0.25$ and salt concentration $\kappa a = 0.2$. The inset shows the points of electroneutrality of the complexes (black disks) together with a zoom onto the $vc_{1,0} = vc_{0,1} = 10^{-12}$ case.

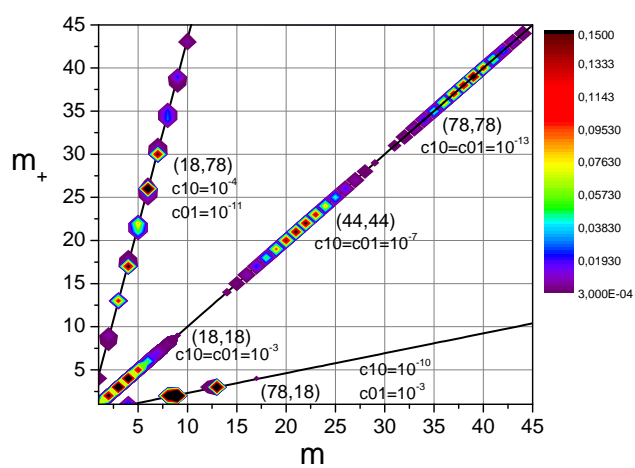


Fig. 13 Projections of the probability distribution function (normalized vc_{m_+,m_-}) on the plane (m_+, m_-) for different lengths of block copolymers of opposite charge with the same distance between the charges, $\xi = 0.25$ and $\kappa a = 0.2$. Increasing concentrations of individual chains, $vc_{1,0}$ and $vc_{0,1}$, increases the aggregation numbers, which move along the electroneutrality lines.

ative correlation energy³⁶.

Summary of main notations used

q	elementary charge
a	Kuhn length, assumed equal for both polycationic and polyanionic chains
z_{\pm}	total charge of a chain, in units of $\pm q$
n_{\pm}	distance between $\pm q$ charges along a linear polymer, in units of Kuhn length
N	length of a neutral polymer block, in units of the Kuhn length
m_{\pm}	number of positive/negative chains in an aggregate (core)
ℓ_B	Bjerrum length $q^2/(\epsilon kT)$ defined from temperature and solvent dielectric permittivity
R_c	radius of a spherical aggregate/core
Z_1	bare charge of a spherical core (due to polymers)
Z_2	“uptake” charge of a core (due to polymers and salt ions inside the core)
Z_3	effective (or renormalized) charge of a spherical core, relevant at large distances from the core center
\tilde{Z}	reduced charge, defined as $\tilde{Z} = Z\ell_B/R_c$
c_{∞}	salt density in the reservoir
κ^{-1}	Debye length, defined through $\kappa^2 = 8\pi\ell_B c_{\infty}$
$\rho(r)$	total density of charge at a distance r from core center
ρ_c	parameter controlling the charge of the corona (case B)
ξ	Manning parameter defined as $\lambda_{\pm}\ell_B \propto \ell_B/n_{\pm}$, where λ_{\pm} is the linear charge of a linear polymer

Acknowledgments

We would like to thank A. Chepelianskii, F. Closa and E. Raphael for useful discussions.

References

- 1 A. V. Kabanov and V. A. Kabanov, *Bioconjug. Chem.*, 1995, **6**, 7–20.
- 2 L. Bromberg, S. Deshmukh, M. Temchenko, L. Iourtchenko, V. Alakhov, C. Alvarez-Lorenzo, R. Barreiro-Iglesias, A. Concheiro and T. A. Hatton, *Bioconjug. Chem.*, 2005, **16**, 626–633.
- 3 N. Lefevre, C.-A. Fustin and J.-F. Gohy, *Macromol. Rapid Commun.*, 2009, **30**, 1871–1888.
- 4 M. A. I. W. A. Seitz and A. T. Balaban, *Curr. Pharm. Des.*, 2002, **8**, 2441–2473.
- 5 K. T. Oh, T. K. Bronich, L. Bromberg, T. A. Hatton and A. V. Kabanov, *J. Control. Rel.*, 2006, **115**, 9–17.
- 6 A. V. Kabanov and V. A. Kabanov, *Adv. Drug Del. Rev.*, 1998, **30**, 49–60.
- 7 K. Kataoka, A. Harada and Y. Nagasaki, *Adv. Drug Del. Rev.*, 2001, **47**, 113–131.
- 8 A. Harada and K. Kataoka, *Science*, 1999, **283**, 65–67.
- 9 E. R. Gillies and J. M. J. Frechet, *Pure Appl. Chem.*, 2004, **76**, 1295–1307.
- 10 A. V. Kabanov, S. V. Vinogradov, Y. G. Suzdaltseva and V. Y. Alakhov, *Bioconjug. Chem.*, 1995, **6**, 639–643.
- 11 J. Zhang, Y. Zhou, Z. Zhu, Z. Ge and S. Liu, *Macromolecules*, 2008, **41**, 1444–1454.
- 12 M. Burkhardt, M. Ruppel, S. Tea, M. Drechsler, R. Schweins, D. V. Pergushev, M. Gradzielski, A. B. Zevin and A. H. E. Muller, *Langmuir*, 2008, **24**, 1769–1777.
- 13 T. Etrych, L. Leclercq, M. Boustta and M. Vert, *Eur. J. Pharm. Sci.*, 2005, **25**, 281–288.
- 14 V. V. Vasilevskaya, L. Leclercq, M. Boustta, M. Vert and A. R. Khokhlov, *Macromolecules*, 2007, **40**, 5934–5940.
- 15 A. V. Kabanov, T. K. Bronich, V. A. Kabanov, K. Yu and A. Eisenberg, *Macromolecules*, 1996, **29**, 6797–6802.
- 16 J. V. M. Weaver, S. P. Armes and S. Liu, *Macromolecules*, 2003, **36**, 9994–9998.
- 17 I. K. Voets, A. de Keizer, F. A. Leermakers, A. Debuigne, R. Jerome, C. Detrembleur and M. A. C. Stuart, *Eur. Pol. J.*, 2009, **45**, 2913–2925.
- 18 E. S. Dragan and S. Schwarz, *J. Polym. Sci. A: Polym. Chem.*, 2004, **42**, 2495–2505.
- 19 E. S. Dragan, M. Mihai and S. Schwarz, *Coll. and Surf. A: Physicochem. Eng. Aspects*, 2006, **290**, 213–221.
- 20 A. Harada and K. Kataoka, *Macromolecules*, 1998, **31**, 288–294.
- 21 A. Kudlay, A. V. Ermoshkin and M. O. de la Cruz, *Macromolecules*, 2004, **37**, 9231–9241.
- 22 A. Kudlay and M. O. de la Cruz, *J. Chem. Phys.*, 2004, **120**, 404–412.
- 23 P. G. Higgs and J.-F. Joanny, *J. Chem. Phys.*, 1991, **94**, 1543–1554.
- 24 E. S. Lee, K. T. Oh, D. Kim, Y. S. Youn and Y. H. Bae, *J. Control. Rel.*, 2007, **123**, 19–26.
- 25 E. Y. Kramarenko, A. R. Khokhlov and P. Reineker, *J. Chem. Phys.*, 2003, **119**, 4945–4952.
- 26 E. Y. Kramarenko, A. R. Khokhlov and P. Reineker, *J. Chem. Phys.*, 2006, **125**, 194902.
- 27 L. Xu, Z. Zhu, O. V. Borisov, E. B. Zhulina and S. A. Sukhishvili, *Phys. Rev. Lett.*, 2009, **103**, 118301.
- 28 O. V. Borisov and E. B. Zhulina, *Macromolecules*, 2002, **35**, 4472–4480.
- 29 M. Castelnovo, *Europhys. Lett.*, 2003, **62**, 841–847.
- 30 P. Sens, C. M. Marques and J.-F. Joanny, *Macromolecules*, 1996, **29**, 4880–4890.
- 31 D. Izzo and C. M. Marques, *J. Phys. Chem. B*, 2005, **109**, 6140–6145.
- 32 V. A. Baulin, A. Johnner and J. Bonet-Avalos, *J. Chem. Phys.*, 2010, **133**, 174905.
- 33 E. Trizac, L. Bocquet and M. Aubouy, *Phys. Rev. Lett.*, 2002, **89**, 248301.
- 34 P. S. Chelushkin, E. A. Lysenko, T. K. Bronich, A. Eisenberg, V. A. Kabanov and A. V. Kabanov, *J. Phys. Chem. B*, 2008, **112**, 7732–7738.
- 35 K. Wu, L. Shi, W. Zhang, Y. An, X.-X. Zhu, X. Zhang and Z. Li, *Soft Matter*, 2005, **1**, 455–459.
- 36 Y. Levin, *Rep. Prog. Phys.*, 2002, **65**, 1577.
- 37 E. Trizac, *Phys. Rev. E*, 2000, **62**, R1465–R1468.
- 38 E. Trizac, L. Bocquet, M. Aubouy and H. H. von Grunberg, *Langmuir*, 2003, **19**, 4027–4033.
- 39 A. Chepelianskii, F. Mohammad-Rafiee, E. Trizac and E. Raphael, *J. Phys. Chem. B*, 2009, **113**, 3743–3749.
- 40 E. Trizac and J.-P. Hansen, *Phys. Rev. E*, 1997, **56**, 3137–3149.
- 41 E. Trizac and G. Tellez, *Phys. Rev. Lett.*, 2006, **96**, 038302.
- 42 B. Duplantier, *J. Stat. Phys.*, 1989, **54**, 581–680.
- 43 H.-P. Hsu, W. Nadler and P. Grassberger, *Macromolecules*, 2004, **37**, 4658–4663.
- 44 M. Rubinstein and R. H. Colby, *Polymer Physics*, Oxford University Press, 2003.
- 45 I. A. Nyrkova and A. N. Semenov, *Faraday Discuss.*, 2005, **128**, 113–127.
- 46 A. Chepelianskii, F. Closa, E. Raphael and E. Trizac, *EPL*, 2011, **94**, 68010.